Comparative study of a cubic, Kelvin and Weaire-Phelan unit cell for the prediction of the thermal conductivity of low density silica aerogels

Steven K. Latré, Steve De Pooter, Dermot Brabazon, David Seveno, Frederik Desplentere

Research Group ProPoliS, KU Leuven Bruges Campus, Bruges, Belgium
Department of Materials Engineering, KU Leuven, Leuven, Belgium
I-Form, Advanced Manufacturing Research Centre, And Advanced Processing Technology Research Centre, School of Mechanical and Manufacturing Engineering, Dublin City University, Dublin, Ireland

Abstract

Super insulating porous materials such as silica aerogels have remarkable thermal insulating properties as demonstrated, experimentally. However, unravelling the underlying heat transfer phenomena is difficult because of the complex multiscale 3D structure of aerogels. For densities higher than $150 \, \text{kg.m}^{-3}$, there is a good correlation between experimental and predicted thermal conductivity values based on cubic unit cells. However, below $150 \, \text{kg.m}^{-3}$, large discrepancies between measured and predicted thermal conductivity values still exist. This numerical study tackles this issue by predicting thermal conductivities of silica aerogels including solid, gaseous and radiative heat transfers using more representative shaped unit cell types (Kelvin and Weaire – Phelan cells). The effects of the pore size distribution and their shape could then be analyzed. A parametric study was carried out including the skeleton and neck size, the gas void dimension and the contact length between the beads with respect to the density and was benchmarked against available literature. For the investigated range of densities, good agreement was found between the predicted results obtained using these newly applied unit cell geometries and previously measured experimental data.

Keywords: Thermal, Conductivity, Aerogel, Kelvin, Weaire-phelan

1. Introduction

The reduction of energy consumption is an important goal in the civil construction sector. Building energy consumption increased by 41.1% between 1980 and 2010 in the U.S. and is still increasing [1]. Consequently, there is a strong demand for new insulation materials. Widely used construction materials such as concrete or plaster typically possess high thermal conductivities in the range of $1-10 \text{ W m}^{-1} \text{K}^{-1}$ which do not provide sufficient thermal resistance for heat transfer. From a thermal performance perspective, adding super insulating materials in an appropriate way can decrease the total thermal conductivity up to one order of magnitude [2]. These types of insulating materials have an effective thermal conductivity lower than that of quiescent air ($0.025 \text{ W m}^{-1} \text{K}^{-1}$ [3]) at room temperature. Silica aerogels, the first material produced as an aerogel [4], typically consisting of a nanoporous network of silicon dioxide particles [5], have lower thermal conductivities values and are therefore one of the most promising construction additives. Their low thermal conductivity is a consequence of their structure which can be described as a mesoporous structure with a randomly arranged low volume fraction of silica (skeletal pearl necklace structure) and a large volume fraction of mesopores. These silicon dioxide particles are in most of the literature described as secondary particles or beads with a median diameter of 7 nm. These beads consist of a network of individual silicon and dioxide atoms interconnected to each other in a complex non regular structure. This work focuses on the mesoscale geometrical representation and the prediction of the thermal conductivity at bead level. The investigated beads, as described in Ref. [5], possess a certain overlap or relative contact length between their neighbors which is typically between 0.3 and 0.9 (30–90%). The existing gaseous pores, between these backbones, formed during the sol-gel process, typically, have dimensions of 10–100 nm [6]. These two geometric characteristics are responsible for the low bulk densities (up to 3 kg m^{-3}) and the high specific surface areas. The present study focusses on the effects of these intrinsic geometrical parameters on the thermal conductivity including solid and gaseous conduction as well as radiation (without coupling effects) by use of finite element simulations in a continuum approach. Roberts et al. [7] used an intersection volume of two independent two-level cut Gaussian random fields as a finite element mesh to represent a polymeric and colloidal aerogel. For more realistic structures at the nanoscale, Molecular Dynamics (MD) simulations [8] can be used and the resulting structures can be converted into representative meshes for finite element simulations. Others [9] performed a complex Monte-Carlo simulation of cluster-cluster aggregation in the Epstein regime with included particle motions and structure growth based on different kinetic exponents. The main characteristics of the proposed unit cell structures in this work, which are based on foams, are used to set-up a tetrahedral element mesh for use in finite element simulations. However, it has been concluded previously that the prediction of the thermal conductivity of silica aerogels based on a simple cubic unit cell model could already be reliable and moreover required limited computational resources compared to the approaches listed above [2]. The results, on the other hand, were only valid for high densities ($\rho > 150 \text{ kg.m}^{-3}$) because of the pore size distribution effect which indicates the presence of randomly distributed larger, is of minor importance. The Kelvin and Weaire-Phelan unit cells, however, bring relief on this aspect as they mimic more closely the structure of real aerogel pores. The presence of dead ends, lost edges and randomness, found in real aerogels has not yet been well examined. These assumptions will have their influences but were not yet estimated in this work. The values for the thermal conductivity were benchmarked against available experimental values obtained from literature for a density ρ between 80 kg m^{-3} and 120 kg m^{-3} [2]. In addition, a comprehensive parametric study was carried out to investigate

the individual influences of geometric parameters such as skeletal bead dimensions and neck sizes, contact length between the beads and void dimensions as a function of the aerogel density.

2. Method

A real silica aerogel structure at its intrinsic dimensions consists of a network of individual silicon and dioxide atoms (at Angstrom scale) interconnected to each other in complex non regular structure (Fig. 1). This structure depends on the production process. Particularly, the presence of free hydrogen bonds (pH) in a solution in the sol-gel process strongly influences the structure [6]. It starts with a solution of (nearly) solid SiO_2 particles dispersed in water, if water glass was used, or alcohol in case of TMOS or TEOS (TMOS: tetramethyl orthosilicate $Si(OCH_3)_4$ and TEOS: tetraethyl orthosilicate - $Si(OC_2H_5)_4$). The pH of the solution determines whether the skeleton is likely to consist of long or short backbones (in case of low pH ($\approx$2–5) or short (pH $\approx$ 7–10)). It influences the dimensions of the skeleton of the backbone and the distribution of the pores. In the case of a low pH, the groups at the end of the formed oligomer are most reactive. Consequently, long backbones are formed. This formation pursues until a full 3D structure is formed, typically with small beads and small air pores due to the polymerization of the silicic acid in the acidic solution. In the case of a higher pH, between 7 and 10, only the mid regions of the oligomers are reactive. In that case, the silica polymerizes to discrete spherical like beads with larger pore dimensions. Normally, a pH is of between 4 and 8 is considered. In some cases, if water glass is used, an ion exchange precedes to start at a lower pH (e.g. 2), with extra addition of silicic acid [6]. Then, a base is added to start the branching of the solid backbone. In fact, this sol-gel process inherently influences the thermal performance as the thermal conductivity is strongly depending on the structure as indicated later in this work by the simulation results. The porosity, which can be up to 99%, is a consequence of the formed type of skeletal backbone and the space between these backbones. We assume at this point in time the spherical beads to be solid silica (Fig. 1, middle figure).
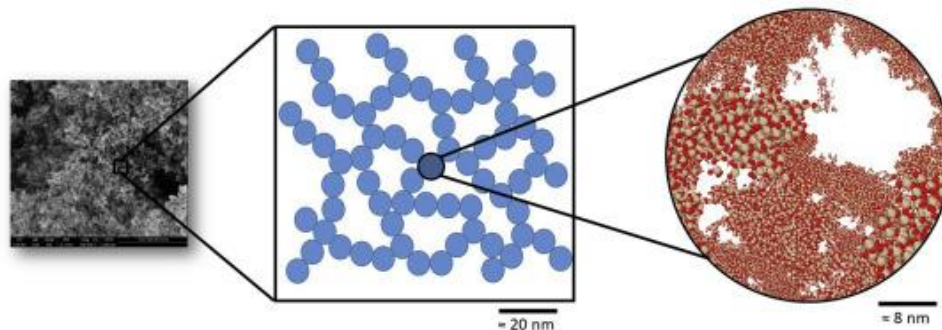

Fig. 1. Schematic representation of the used top-down approach: SEM image of an aerogel processed by Ref. [6](left), schematic picture to depict the bead structure at meso level (middle) and an image of an aerogel structure at nano level (right).

The possible heat transfer mechanisms in silica aerogel at the nanoscale include solid and gaseous conduction and radiation. Here, the predicted thermal conductivities comprise these mechanisms without coupling, which will lead to an underestimation of the total effective thermal conductivity [10]. No convection is included, since the aerogel pore sizes are typically less than 500 nm and no convection occurs below 4 mm [[11], [12], [13]]. The solid and gaseous conduction as well as radiation was evaluated based on the geometrical dimensions and the existing literature. The effective (macro scale) thermal conductivity was then determined by finite elements simulations and Fourier's law (Eq (1)) [14]:

$$\dot{Q} = \lambda A \frac{\Delta T}{e} \tag{1}$$

here $\dot{Q}$ is the heat flow rate [W], λ, the thermal conductivity [W.m^{-1}.K^{-1}], A, the area through which the thermal flow diffuses [m^2](Fig. 3), e, the dimension of unit cell [m] in the direction of the heat flow (Fig. 3) [2] and ΔT, the temperature difference between the two applied temperature boundary constraints [K]. The individual local temperature gradients per volume ΔT were determined by use of steady state finite volume simulations described later in this work. Since the total temperature difference is fixed and A and e are known, the total effective thermal conductivity can be determined by calculation of $\dot{Q}$. In the following paragraphs, the individual analytical calculations for the solid, gaseous and radiative conduction values are summarized. Also, the influences of the intrinsic dimensions and the different types of heat transfer with respect to the aerogel density are discussed.

2.1. Calculation of the solid conduction in the aerogel backbone

Due to the amorphous structure of aerogel, the heat transfer depends strongly on the thermal conductivity of the solid backbone [15] and consequently the localized atomic vibrations. These movements are limited by atom scattering at a distance corresponding to the inter-atomic spacing. The thermal conductivity can be calculated by the sum of three Debye integrals [16] which depend on the velocity of sound in the pores. However, the use of the work of Cahill et al. requires a correction for the damping of the sound velocity by the ratio of the atomic density given by Hopkins et al. [17]. The most appropriate formula, to our knowledge, depends again on the average inter-atomic spacing but can be calculated by use of the kinetic theory which describes the relation between the thermal resistance of the backbone and its inter-atomic spacing [15] and includes the volumetric aspect of the velocity of sound in the pores. Combining this theory and the Matthiessen's rule [18] gives:

$$\lambda_s = \tfrac{1}{3} C_v v_0 \Lambda_0 \tag{2}$$

with λ_s, the thermal conductivity of the aerogel backbone, C_v, the volumetric specific heat, v_o, the mean sound velocity of the aerogel backbone and Λ_0, the average inter-atomic spacing in the aerogel backbone. The value of Λ_0 for the interfacial contact of the individual beads on the skeleton can be calculated from the volumetric resistance, transmission resistance and space resistance (Λ_V, Λ_S & Λ_T respectively) [15]:

$$\frac{1}{\Lambda_0} = \frac{1}{\Lambda_V} + \frac{1}{\Lambda_S} + \frac{1}{\Lambda_T} \tag{3}$$

Each term in this formula can be calculated individually and depends on the assumed bead diameter d_p and pitch between the beads. We refer to Ref. [15,19] for more detailed calculations dependent on the overlap a/d_p, Fig. 2. Different bead diameters d_p (4, 6 and 8 nm) and overlap ratios of a/d_p (0.45, 0.5, 0.6, 0.7, 0.8) were used. The values for Λ_V, Λ_S & Λ_T for an overlap of 0.7 and a bead diameter of 4 nm are summarized in Table 1.

(a)   (b)
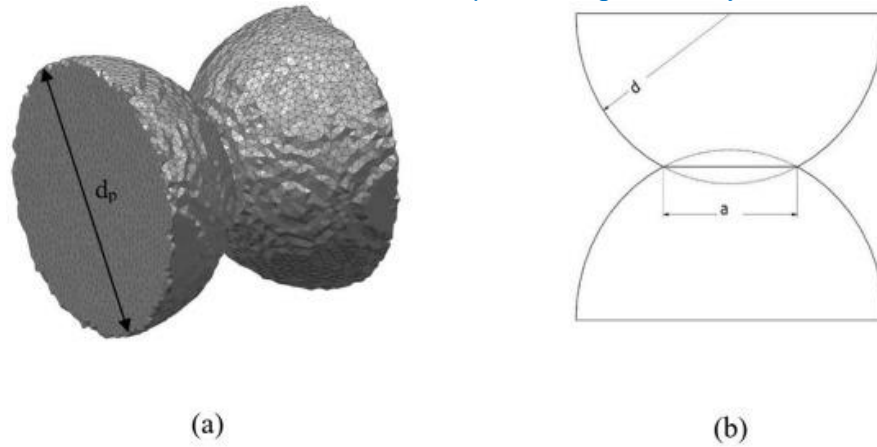
Fig. 2. Representation of an overlap (= a/d_p) of 0.3 between two adjacent backbone spheres.

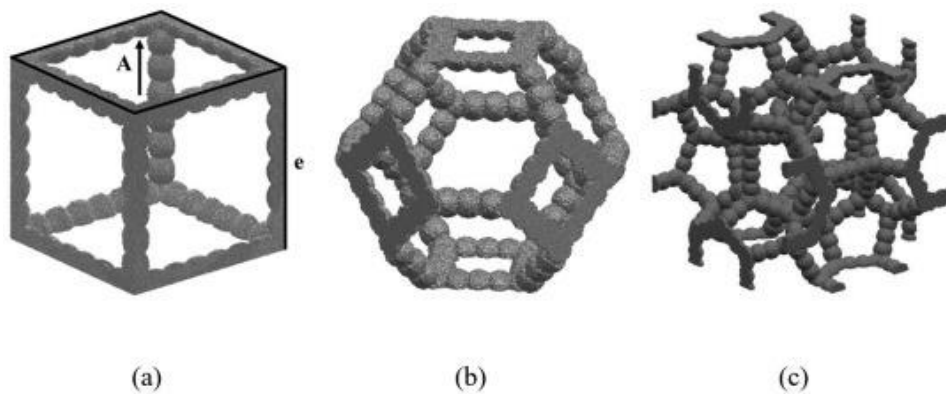(a)   (b)   (c)

Fig. 3. Simulation unit cell representation: a cubic cell (a), a Kelvin cell (b) and a Weaire-Phelan cell (c).

Table 1. Values for the thermal conductivity of the backbone due to volumetric, transmission and space resistance for bead diameters of 4 nm and 8 nm with an overlap of 0.7.

d_p	a/d_p	A_{inter} (nm²)	Λ_S (nm)	Λ_V (nm)	Λ_T (nm)	Λ_0 (nm)	λ_0 (W.m⁻¹.K⁻¹)
4	0.70	6.15	3.61	0.56	1.05	0.33	0.818
8	0.70	24.6	7.21	0.56	2.09	0.42	1.027

In Fig. 4, the estimation of the thermal conductivity of the aerogel backbone is shown as a function of the bead diameter (d_p: 2–10 nm) and an overlap (0.1–0.9). The bigger the particle diameter, the larger the influence of the overlap. This is in agreement with previous report [15]. The solid thermal conductivity of an aerogel backbone with bead diameter of 4 nm and an overlap of 0.4 is 0.36 W m⁻¹ K⁻¹, while for an overlap of 0.8 the solid thermal conductivity is 0.72 W m⁻¹ K⁻¹. For a bead diameter of 8 nm, values of 0.44 and 0.93 W m⁻¹ K⁻¹ are obtained for an overlap of 0.4 and 0.8 respectively. Consequently, the overlap becomes more important for larger bead diameters. This can be explained by the change of the interatomic spacing which becomes larger if the bead diameter is larger. Then, while the volumetric resistance is taken as constant [19], the interatomic spacing due to space and transmission resistances are higher too, which lead to a higher inter-atomic spacing in general. From Eq (2), we know that an increase in thermal conductivity is due to the bigger interface area between the beads.
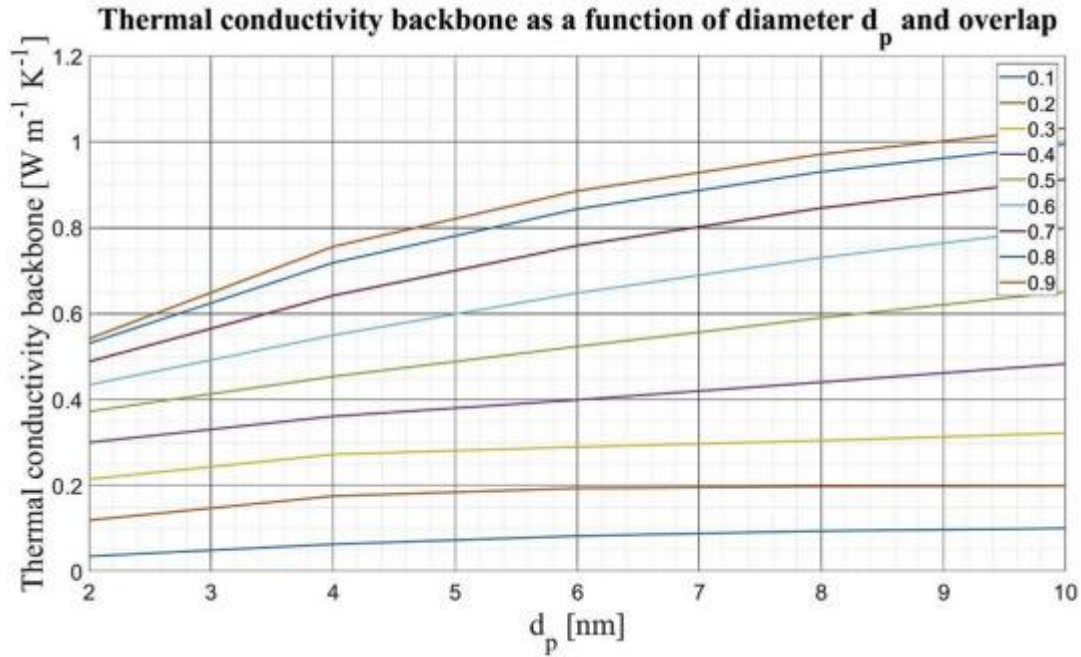
Fig. 4. Thermal conductivity of the backbone as a function of particle diameter ranging from 2 to 10 nm and an overlap ranging from 0.1 to 0.9.

2.2. Calculation of the gaseous conduction in the voids of aerogel

The gaseous conductivity is calculated by use of Kaganer's model [20]:

$$\lambda_g = \frac{\lambda_{air}}{1+2\beta K_n} \tag{4}$$

where λ_g, the gaseous thermal conductivity [W.m^{-1}.K^{-1}], λ_{air}, the thermal conductivity of free air (= 0.025 W m^{-1} K^{-1}), β, a coefficient depending on the adiabatic and accommodation coefficient of air ($\beta \approx 1.55$ [21]) and K_n, the Knudsen number. The Knudsen number is the ratio of the (air) mean free path to the pore size (D in Fig. 5) [22]:(5)Kn=kBT2πdp2pL

$$K_n = \frac{k_B T}{\sqrt{2}\pi d_p^2 pL} \tag{5}$$

where k_B is the Boltzmann constant ($k_B = 1.38 \times 10^{-23}$ m^2 kg s^{-2}.K^{-1}), T, the temperature (K), d_p, the particle diameter [m], p the pressure (Pa) and L, the mean free path travelled by a particle between two successive collisions with other particles. Different solid backbone diameters and overlaps were modelled with densities ranging from 70 till 120 kg m^{-3}. In Fig. 6, a 3D view of the gaseous phase of a Kelvin unit cell is depicted. The density of the unit cell model can be modified by changing, inter alia, the distance D (Fig. 5). For each D, the value for the gaseous thermal conductivity was calculated (Fig. 7). There is a sub-linear relation between the thermal gaseous conductivity and void dimension D. However, for low density aerogels, the value of the gaseous conductivity becomes important, certainly for

example for $D > 80$ nm. For example, for $\rho = 83$ kg m^{-3}, $d_p = 8$ nm, $a/d_p = 0.7$ and $D = 85$ nm, λ_g is 0.0059 W m^{-1} K^{-1}.
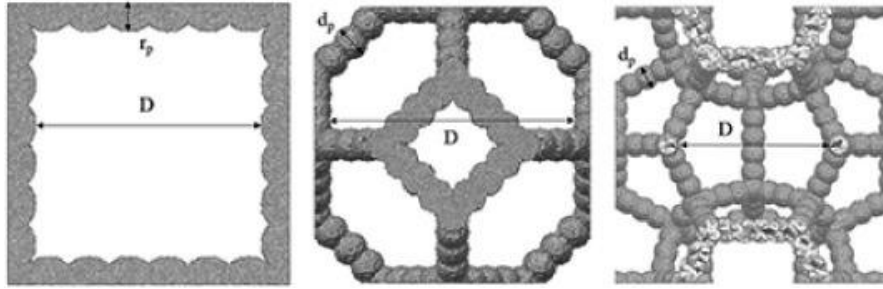

Fig. 5. Schematic representation of the dimensions D and d_p used to calculate the thermal gaseous conductivity in case of a cubic, a Kelvin and a Weaire-Phelan unit cell (from left to right respectively).
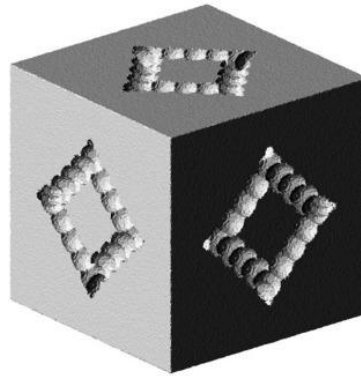

Fig. 6. 3D view of the gaseous phase in a Kelvin unit cell simulation model.
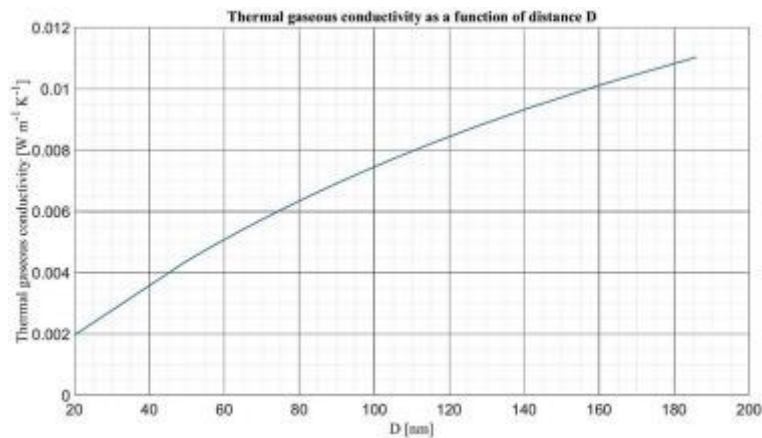

Fig. 7. Thermal gaseous conductivity as a function of void dimension D.

2.3. Calculation of the radiative heat transfer in voids

The radiative heat transfer can be calculated using different methods as Discrete Dipole Approximation [23], multi-sphere T-matrix method [24,26] or the Rossland and Mie theory [27]. Based on [[27], [28], [29], [30]], the radiative thermal conductivity was calculated by the following expression:

$$\lambda_r = \frac{16n^2\sigma T^3}{3\beta}$$ (6)

where n is the average refractive index of silica aerogels, σ, the Stefan-Boltzmann constant ($\sigma = 5.67 \times 10^{-8}$ J s^{-1} m^{-2}.K^{-4}), T, the temperature [K] and β the temperature dependent Rossland extinction coefficient [26]. n can be calculated with the Henning and Svensson relation, Hartmann or Philipp method [31]. Enguehard et al. [26] proposed a fix value of 1.04 for n justified by the work of [32] which is used here as well. The Rossland extinction coefficient β was calculated by use of the average method based on measurements carried out with infra-red spectroscopy [33]. This coefficient β can also be rewritten into $\rho \cdot e$ with the density ρ and the Rossland extinction e. For different densities (70 kg m^{-3} - 120 kg m^{-3}, Fig. 8), the Rossland extinction e was taken constant [33] as all studies were performed for a fixed boundary temperature of 300K which corresponds to a range of 3500–9000 m^{-1} for β. Applying Eq (6), λr lies between 0.0025 W m^{-1} K^{-1} and 0.00098 W m^{-1} K^{-1}. This value was included in the calculation of total effective thermal conductivity as an additional value without considering a coupling effect.
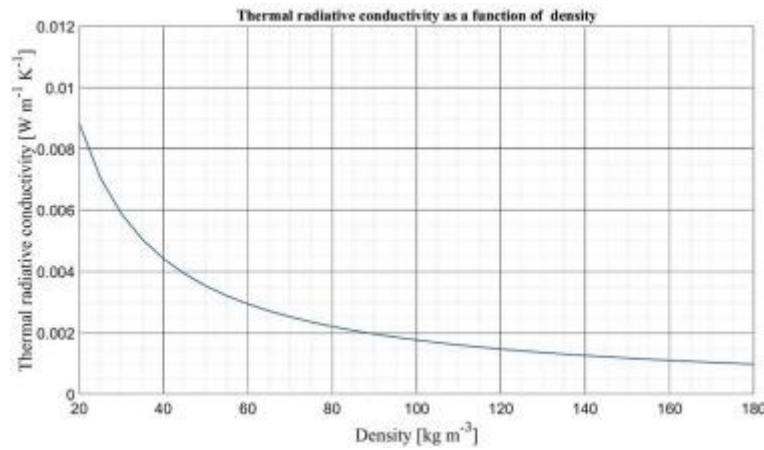

Fig. 8. Radiative thermal conductivity as a function of density.

2.4. Calculation of the density versus intrinsic dimensions d_p and D

The correlation between the parameters d_p, D and the density has been thoroughly experimentally investigated in Ref. [34,35]. Measurements for bead diameter, porosity and density have been correlated and fitted into the following widely accepted expressions:

$$D \approx \frac{4V_{pore}}{S_{ext}}$$ (7)

$$d_p = \frac{6}{S_{ext}\rho_s}$$ (8)

$$V_{pore} \approx \frac{1}{\rho} - \frac{1}{\rho_s}$$ (9)

where D is the void dimension [nm], V_{pore}, the pore volume, S_{ext}, the external specific surface area [m^2.kg], d_p, the bead diameter and ρ_s, the density of the solid backbone

[kg.m^{-3}]. Combining equations (7), (8), (9)), the 'state-of-the-art' empirical relation between D, d_p and the density can be rewritten as follows [15]:

$$D = \frac{4}{\frac{\delta}{\rho_s d_p}}\left(\frac{1}{\rho} - \frac{1}{\rho_s}\right) \tag{10}$$

If ρ_s is known (in this work, as mentioned, the beads are considered full silica, $\rho_s = 2278$ kg m^{-3} [15]), Eq (10) can be rearranged to calculate the appropriate density as a function of the dimensions D and d_p. Eq. (10) can then propose a first estimation of D and d_p for a certain density considering no specific overlap between the beads. A similar approach is used in Refs. [10,22,33,36,37] where the geometrical parameters D and d_p are mathematically defined from the measured specific surface S and the aerogel's porosity φ_{ae}. With respect to this work, Wei et al. [33] state that the cubic unit cell is a useful and a simple representative unit cell (RUC) for an aerogel with mesoscale dimensions $d_p \sim 2$–5 nm and $D \sim 10$–50 nm or in terms of density, higher than 120 kg m^{-3}. In Refs. [10], different types of unit cells were benchmarked against these cubic unit cell based simulations to estimate the pore size distribution effect and the shape of the backbone structure. The proposed models were generated to meet different densities by using Eq (10). In this work, this approach was extended to new types of representative unit cell types such as Kelvin and Weaire-Phelan cells. The total densities were calculated by means of the sum of the individual volume percentages of the tetrahedral elements multiplied by their individual intrinsic densities gas ρ_g and solid ρ_s. The results of the simulations generated effective thermal conductivities for the different proposed models. After addition of the radiative heat transfer, these values were compared to experimental values available in literature to validate the simulations.

2.5. Calculation of the density versus pore size dimension D

The relation between the pore size D and the density was investigated for a fixed bead diameter of 4 nm and is shown for the three types of unit cells in Fig. 9. It is clear that for a certain density ρ, the three unit cells underestimate distance D with respect to Eq (10). However, the curves representing the Kelvin and Weaire-Phelan unit cells are closer to the state-of-the art relation than the cubic unit cell. It is expected that these types will correspond better to the measurements. It is also clear that above 150 kg m^{-3}, the Kelvin and Weaire-Phelan cell would fit the state-of-the art relation much better than the cubic unit cell. It can be calculated that the Kelvin and Weaire-Phelan unit cell would cross the state-of-the-art relation at 225 and 160 kg.m^{-3} respectively. Since the attention is specifically oriented to the densities below 150 kg m^{-3}, no simulations regarding this range of high densities were carried out. Next to this, due to the pore size distribution effect, the values for D are larger at lower densities for real aerogels which is, to our knowledge, for the first demonstrated for foam-like structures. Also, in a previous study [19], at densities below 90 kg m^{-3}, it was challenging to create structures because of geometrical constraints in the corners of the cubic unit cell. As the actual pores are more likely to correspond to a spherical instead of a cubical shape, the Kelvin cell is introduced

which is more or less a draped shape of a sphere while a cubic unit cell has a more deviant bounding box shape. Modelling a sphere like void inside a cubic unit cell led to air filling inner corners [19] and consequently an underestimation of the amount of solid in the unit cell which lowers the density significantly for the same D. In other words, for an identical density, the D value of a Kelvin cell is larger with respect to the cubic unit cell. For this reason, the Kelvin cell is a more representative model than a cubic unit cell and hence gains lower deviations from the state-of-the-art relation. Consequently, for a Kelvin cell, for the same d_p, it is possible to go higher in D while keeping the density constant. Since aerogel structures possess not only sphere like voids, but also a randomly organized branched backbone network, a Weaire-Phelan cell, next to the Kelvin cell, was introduced. All previously described results are not including real aerogel structure characteristics such as dead ends in the branching, localized smaller or bigger bead diameters or cluster forming of the beads.
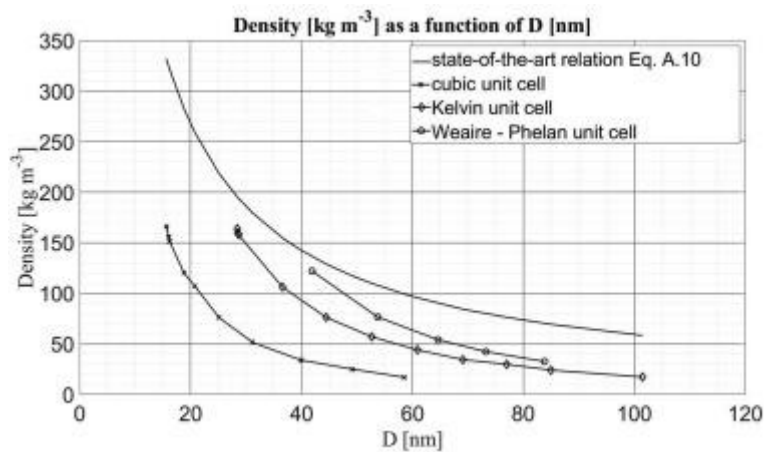

Fig. 9. Aerogel density as a function of void dimension D for the used unit cells and with use of the empiric formula Eq. (10), a fix overlap of 0.7 and a d_p = 4 nm.
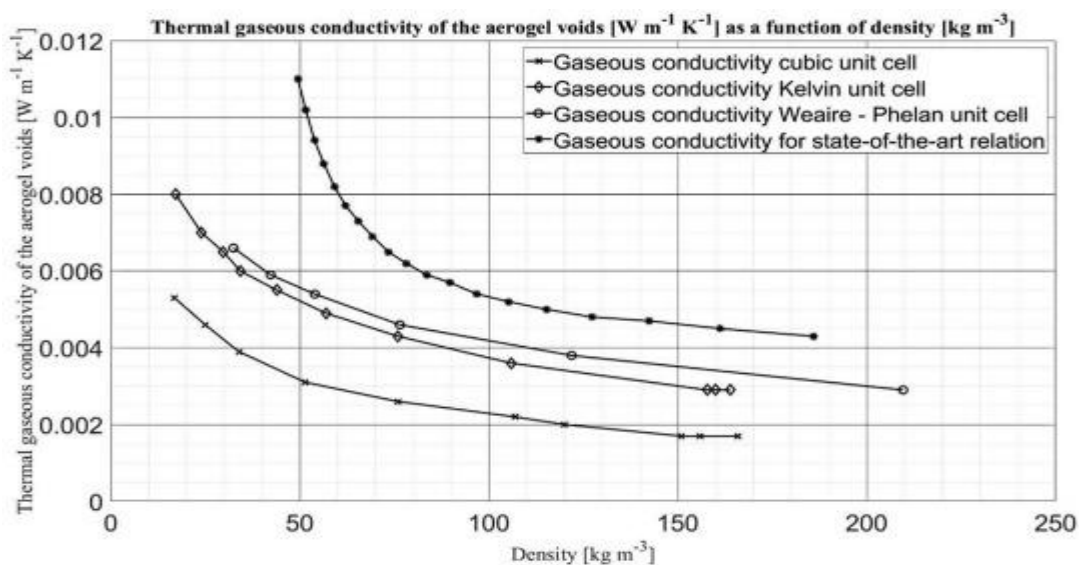

Fig. 10. Thermal gaseous conductivity of the aerogel voids as a function of density for the different unit cell types

2.6. Calculation of the density versus gaseous conductivity

The calculation of the gaseous conduction is primarily linked to the dimension of the void dimension D. For different values of D, the gaseous conductivity was determined from Eq (4) and Eq (5) (Fig. 10). Results for the simulation models based on the cubic, Kelvin and Weaire-Phelan unit cell were included wherein similar values for D are present and compared to real densities. The gaseous conductivity of the Kelvin and Weaire –Phelan unit cell as a function of density is closer to values obtained from Eq (10) than with the cubic unit cell. This result strengthens the choice of the Kelvin and Weaire – Phelan cells as more representative cells to a real aerogel structure than the cubic unit cell.

2.7. Calculation of the density versus radiation

As stated previously, the density is inversely proportional to the radiative heat transfer. Since the mean Rossland extinction coefficient β is high for low densities, the radiative heat transfer is also low for low densities but cannot be neglected as the values can take up to 10–20% of the total effective thermal conductivity in case of aerogels.

2.8. Working principle of the thermal solver

Finite volume simulations were carried out to calculate the thermal flow as in Refs. [19]. The working principle is as follows. To define different materials in one simulation, each individual volume containing that particular material corresponds to a separate 3D mesh. It consists of individual elements labelled by their own density, thermal conductivity and physical properties. Each element is described by its shape and x, y, z – location or centroid location. Hence, the volume is divided into 3D finite volumes. Finite differences are used to approximate the differential increments at any of the coordinates described by dx, dy or dz increments. After applying temperature boundary constraints, in x-direction for example, the temperature gradient is calculated by dividing the temperature difference between x and x + dx (with dx, the element length in x direction) by length dx. If no internal heat generation occurs in the model, a temperature field can be conducted via appropriate Laplace equations and the subsequent partial differential equations. If this finite difference approach is done for all three directions, and the net heat flow into any node should be zero in steady state or equilibrium calculations. Consequently, one can calculate the heat flow of the total mesh in the desired direction(s). In other words, the thermal solver divides the volume or 3D mesh into separate volumes with constant temperature called 'lumps' which have centroids x, y and z. By applying the desired steady state boundary constraints on this lump volume, a 3D matrix of partial differential equations is determined. Proper inverse matrix calculations provide the flux and hence the total thermal conductivity of the model [2].

3. Thermal conductivity simulation details and results

3.1. Simulations details

To generate the structures of the cubic, Kelvin and Weaire-Phelan cell, the correct node center locations of the beads were first located in a 3D environment as a function of the bead diameter d_p, void dimension D and overlap a/d_p. Then, tetrahedral elements were built around these center locations to satisfy the desired geometry conditions and bead shape. The mesh generator relies partially on the iso2mesh tool developed by Ref. [38]. In Fig. 11, Fig. 12, a Kelvin and Weaire-Phelan mesh with different densities are visualized. The developed script also takes into account a desired overlap of 0.7 by growing the whole cell until an error estimation of the overlap satisfies the following range: [overlap - 0.05, overlap + 0.05]. The applied boundary conditions are fixed temperatures on top and bottom of the unit cell with a difference of 2 K. There is no heat transfer occurring on the sides (Fig. 13, red is the highest

temperature, blue is the coldest temperature). The two phases of meshes, solid and gas, are in perfect contact because the nodes of the solid mesh are in perfect contact with the nodes of the gas mesh at the interface. Consequently, the simulation results will overestimate the thermal conductivity as, in reality, a coupling resistance between the solid and gas components is present. This effect has been thoroughly investigated by Refs. [10,36,38] and has a significant contribution to the effective thermal conductivity. However, Bi et al. [10] argued that the thermal conductivity of the air molecules in the gaps of two adjacent particles in the flow direction of the backbone does not vary much due to lattice vibrations of the air molecules. The overestimation is then of minor importance. In contrast to this flow direction, in the perpendicular direction to the backbone, the overestimation is important. This coupling effect can be estimated by analytical calculations but is not included in this parametric study, so the thermal conductivity will certainly be overestimated in this respect.
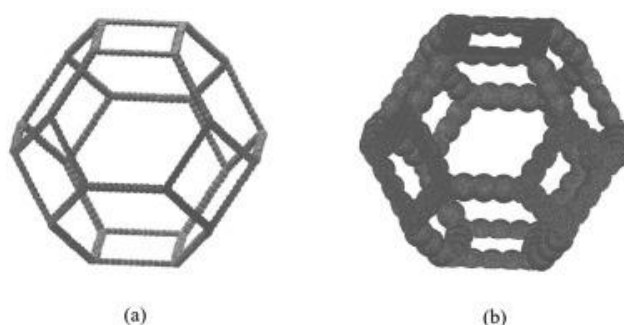

Fig. 11. 3D view of 2 K unit cells with different densities (a: 17.2 kg m^{-3}, b: 164 kg m^{-3}).
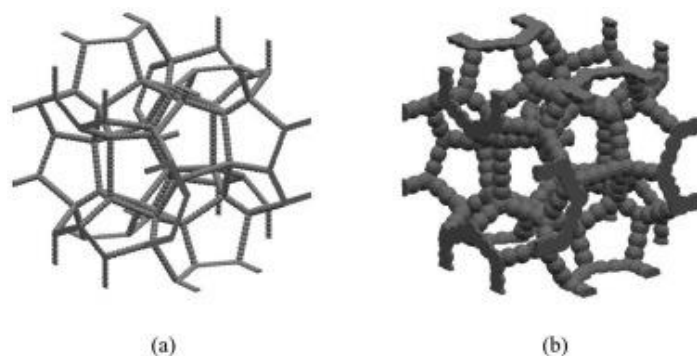

Fig. 12. 3D view of two Weaire-Phelan unit cells with different densities (a: 32.5 kg m^{-3}, b: 209 kg m^{-3}).
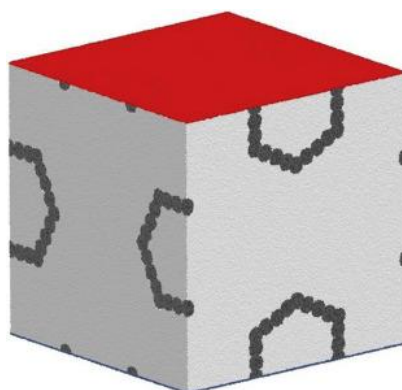

Fig. 13. Representation of the gaseous conduction elements (white) and the solid backbone elements (black) and the two fixed temperature boundary constraints on top and bottom of the Weaire-Phelan unit cell.

3.2. Simulation results

The effects on the aerogel's thermal conductivity including beads with diameters $d_p = 4$, 6 and 8 nm, different void dimensions D and overlap values 0.45, 0.5, 0.6, 0.7 and 0.8, were evaluated (Fig. 14). The values for d_p and D correspond to a density range of 70–120 kg m⁻³. It is clearly visible that the values for the effective thermal conductivity, certainly for low densities, fit well with the Kelvin and Weaire-Phelan unit cells for a bead diameter $d_p = 8$ nm. The cubic unit cell on the other hand, underestimates the effective thermal conductivity (Fig. 15). Consequently, the geometry of the unit cell is therefore important and validated by these simulations. In addition, for very low densities ($\rho < 100$ kg m⁻³), the Weaire-Phelan cell estimates the effective thermal conductivity even better than the Kelvin cell due to the pore size distribution effect which is covered by this type of unit cell.
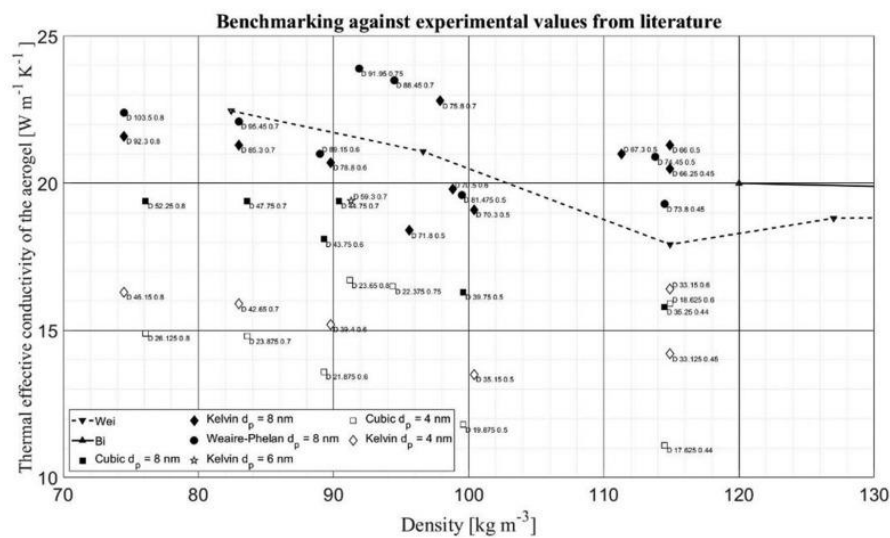

Fig. 14. Comparison between experimental [10,33] and predicted thermal conductivities. Indices give the dimension D and the overlap, e.g. D 46.15 0.8 means a $D = 46.15$ nm and overlap $a/d_p = 0.8$ (for cubic (□), Kelvin (◊) and Weaire-Phelan unit cells (o)).
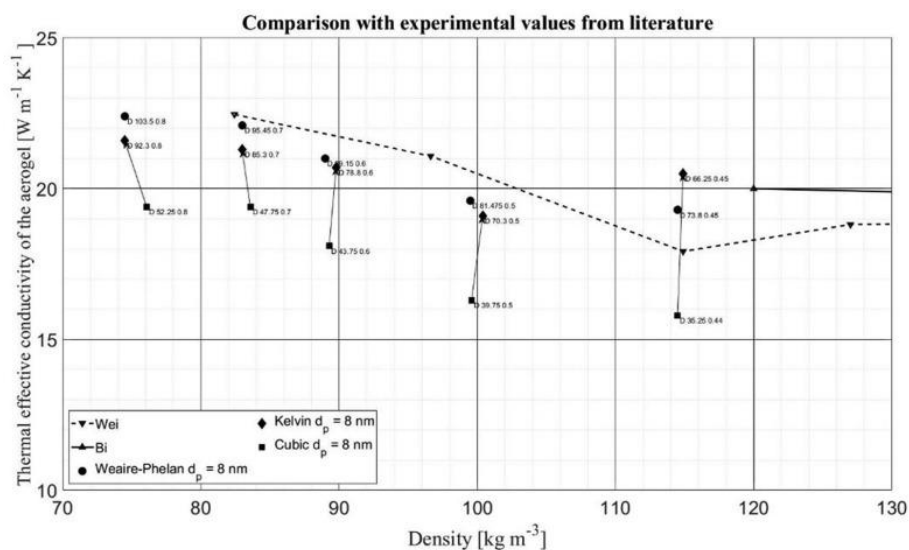

Fig. 15. Underestimation of thermal conductivity between cubic (□), Kelvin (◊) and Weaire-Phelan (o) simulations.

In [39], the authors state that the radiation effect becomes important for insulation materials with small amount of solid content. In addition, when the density increases, the influence of the solid component on the total thermal conductivity increases, while the radiation decreases. Reversely, since radiation is larger for lower densities and the solid backbone becomes more important at higher densities, an optimum is expected where the sum of the contributions from radiation and solid conduction is at a minimum [10,32]. This phenomenon is also visible for the simulations around $100 \, \text{kg m}^{-3}$ for both unit cells and approximately around $115 \, \text{kg m}^{-3}$ for the experiments (Fig. 15). However, in case of Weaire-Phelan cells, the dip is less prominent. To further estimate and investigate the geometrical parameters with respect to the thermal conductivity, an extra series of three different simulations was carried out. Firstly, all values for the predicted thermal conductivity shift upwards vertically towards the experimental values if a bigger bead diameter is proposed. Fig. 16 depicts for example a $d_p = 8$ nm instead of 4 nm while maintaining the overlap, density and shape of the unit cell unchanged. This shift is expected as bigger particle diameters cause an increase in the net overlap A_{inter} and the backbone thermal conductivity. Secondly, if a cubic unit cell is used and only the void dimension D is decreased while keeping the overlap and bead diameter constant, a horizontal shift to higher densities is observed whereas with a Kelvin unit cell, a non-horizontal shift takes place (Fig. 17). Due to the fact that the scaling of a cubic structure is the same in all three dimensions, only a horizontal shift is taking place. The scaling of the Kelvin cell structure, on the contrary, implies a non-equal change in backbone length in all three directions. As the Kelvin cell is more sphere like, the outer backbones are stretched more than the inner. Thirdly, if the density and void dimension D is kept constant together with the bead diameter, a higher overlap shifts the effective thermal conductivity vertically upwards (Fig. 17) because of the nonlinear influence of λ_s as seen in Fig. 6. The results obtained in Fig. 18 are shifted by about $15 \, \text{kg m}^{-3}$ with respect to the experiments. This deviation could be due to the following observations. Firstly, the bead density was set to a fixed value ($2278 \, \text{kg m}^{-3}$) based on the work of [10,15]. This density depends on the intrinsic density of the primary particles. Since they grow in a non-regular structure during the sol-gel process, the density will change and influence the solid backbone density. Secondly, in real aerogels, non-regular shaped structures are formed in contrast to the used Kelvin and Weaire-Phelan cells. Consequently, a real aerogel structure is more likely to be better represented by full random structure with internal branches, dead ends and clustering of the backbones which can influence the local density. Finally, neither one fixed bead diameter nor void dimension D should be used because in real aerogels the bead size and void dimensions are mixed and distributed from small to large. Together with varying overlaps, the density and local thermal conductivity would be influenced. Nonetheless, the impact of these parameters with respect to the total effective thermal conductivity is interesting since these modifications can be directly linked to the production process of an aerogel [6]. In that way, an optimized aerogel targeting a given thermal conductivity range can be produced. Next to this, the simulations are in good agreement with the proposed

literature experiments. It shows that the Kelvin and Weaire-Phelan unit cell can be used to account for size distribution effect thanks to their less regular and more branched shape than a cubic cell.
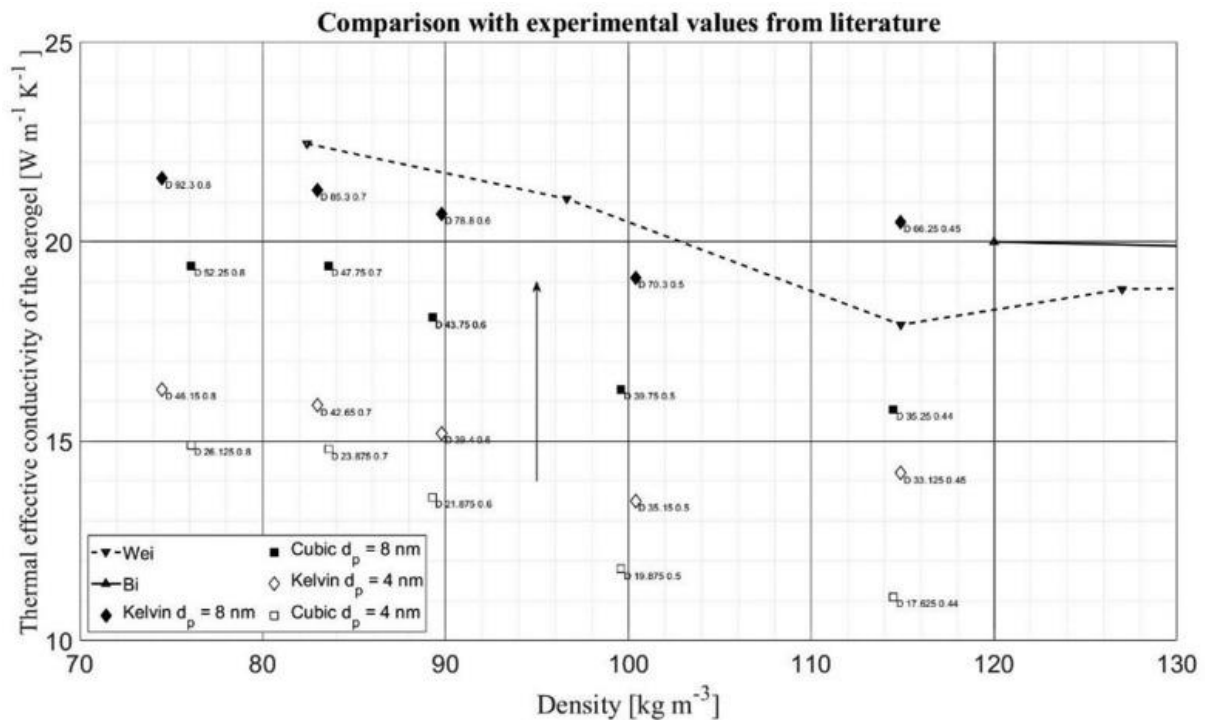

Fig. 16. Effect of a bigger secondary particle diameter while keeping overlap, density and type of the unit cell unchanged.
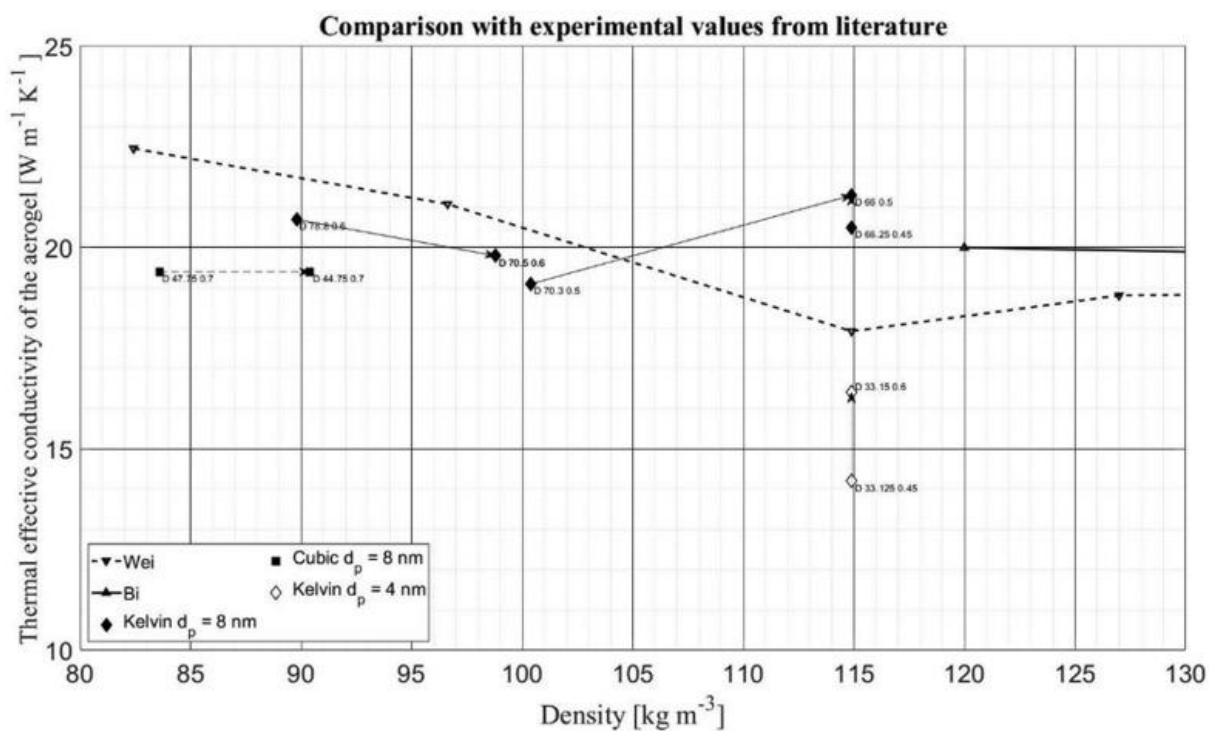

Fig. 17. Shift of the thermal conductivity by changing void dimension D and keeping the overlap and particle diameter unchanged (dashed and full lines). When density

is kept constant together with the particle diameter, a higher overlap shifts the effective thermal conductivity upwards (dotted line).
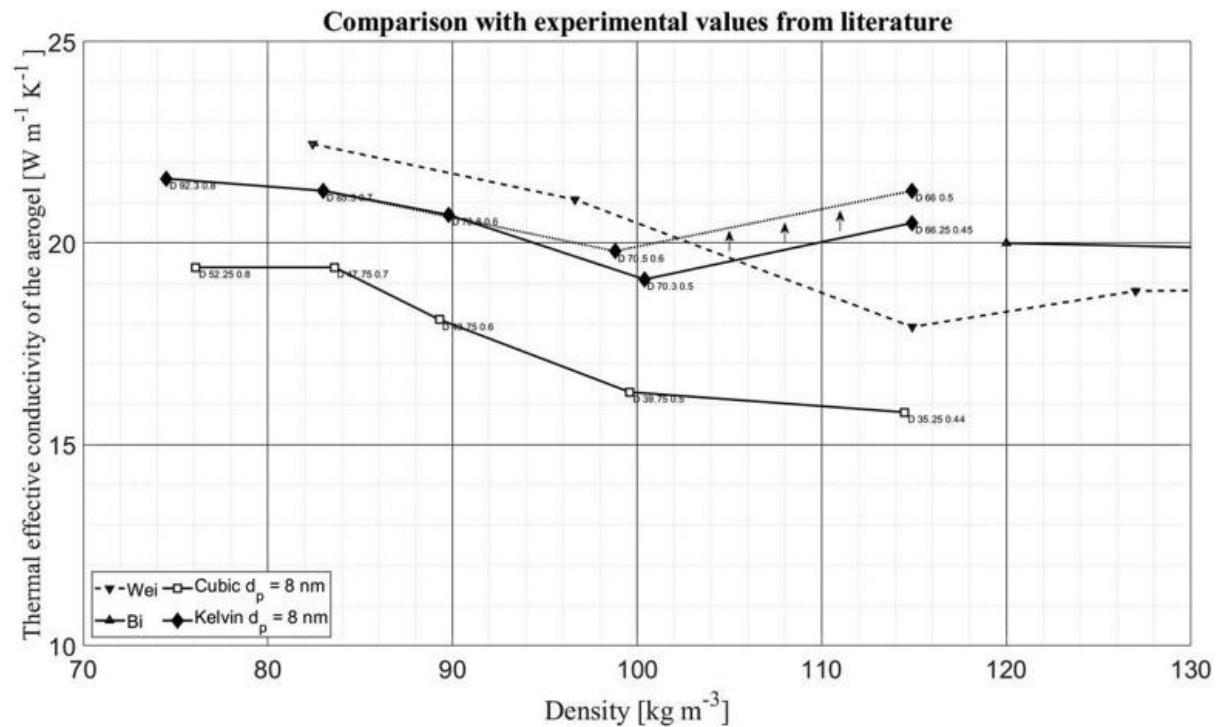

Fig. 18. Shift of the optimum insulation point by keeping a constant particle diameter and overlap and a variable void dimension D.

4. Conclusions

Based on a cubic, Kelvin and Weaire-Phelan cell, analytical calculations combined with finite volume simulations were performed comprising the solid and gaseous conduction and radiation without coupling. The described finite volume simulations include the calculation of the thermal flow through two connected dissimilar meshes. For the different types of unit cells, a parametric study on the effective thermal conductivity of aerogel was carried out to estimate the importance of the shape of the chosen unit cell. It is concluded that below 150 kg.m^{-3}, the cubic unit cell possesses a too regular shape to cope with the random distribution of large pores. The simulations demonstrated that the Kelvin and Weaire-Phelan cell, having less regular shapes and more branched network of solid backbones, can account for this effect thus validating their use for low densities thanks to their less regular shape and more branched network of solid backbones. From an insulation perspective, the parametric study also confirms the existence of an optimum density (100−110 kg m−3) where the sum of the contributions from radiation and solid conduction is at a minimum.

References

[1] X. Cao, X. Dai, J. Liu

Building energy-consumption status worldwide and the state-of-the-art technologies for zero-energy buildings during the past decade
Energy Build., 128 (2016), pp. 198-213, 10.1016/j.enbuild.2016.06.089

[2] S.K. Latre, S. De Pooter, D. Seveno, F. Desplentere

Numerical mesh generation tool for thermal conductivity simulations of nanoparticle filled inorganic plates
Polym. Eng. Sci., 58 (4) (2018), pp. 568-585

[3] D. Baillis, R. Coquard, L.M. Moura

Heat transfer in cellulose-based aerogels: analytical modelling and measurements
Energy, 84 (2015), pp. 732-744, 10.1016/j.energy.2015.03.039

[4] F. Rechberger, M. Niederberger

Synthesis of aerogels: from molecular routes to 3-dimensional nanoparticle assembly
Nanoscale Horizons, 2 (1) (2017), pp. 6-30, 10.1039/c6nh00077k

[5] H. Maleki, L. Durães, A. Portugal

An overview on silica aerogels synthesis and different mechanical reinforcing strategies
J. Non-Cryst. Solids, 385 (2014), pp. 55-74, 10.1016/j.jnoncrysol.2013.10.017

[6] S. De Pooter, S. Latre, F. Desplentere, D. Seveno

Optimized synthesis of ambient pressure dried thermal insulating silica aerogel powder from non-ion exchanged water glass
J. Non-Cryst. Solids, 499 (2018), pp. 217-226, 10.1016/j.jnoncrysol.2018.07.028

[7] A.P. Roberts

Morphology and thermal conductivity of model organic aerogels
Phys. Rev. E, 55 (2) (1997), pp. R1286-R1289

[8] W. Goncalves, J. Morthomas, *et al.*

Elasticity and strength of silica aerogels: a molecular dynamics study on large volumes

Acta Mater., 145 (2018), pp. 165-174

[9] F. Pierce, C.M. Sorensen, A. Chakrabarti

Computer simulation of diffusion-limited cluster-cluster aggregation with an Epstein drag force
Phys. Rev. E - Stat. Nonlinear Soft Matter Phys., 74 (2) (2006), pp. 1-8

[10] C. Bi, G.H. Tang, Z.J. Hu, H.L. Yang, J.N. Li

Coupling model for heat transfer between solid and gas phases in aerogel and experimental investigation
Int. J. Heat Mass Tran., 79 (2014), pp. 126-136, 10.1016/j.ijheatmasstransfer.2014.07.098

[11] Y. Liu

Heat Transfer Mechanism and Thermal Design of Nanoporous Insulating Materials
University of Science and Technology Beijing, Beijing (2007)

[12] L.W. Hrubesh, R.W. Pekala

Thermal properties of organic and inorganic aerogels
J. Mater. Res., 9 (3) (1994), pp. 731-738

[13] P.J. Burns, C.L. Tien

Natural convection in porous media bounded by concentric spheres and horizontal cylinders
Int. J. Heat Mass Tran., 22 (6) (1979)

[14] J.P. Holman

Heat Transfer
(tenth ed.), McGraw-Hill, New York (2009)

[15] C. Bi, G.H. Tang

Effective thermal conductivity of the solid backbone of aerogel
Int. J. Heat Mass Tran., 64 (2013), pp. 452-456, 10.1016/j.ijheatmasstransfer.2013.04.053

[16] D.G. Cahill, S.K. Watson, R.O. Pohl

Lower limit to the thermal conductivity of disordered crystals
Phys. Rev. B, 46 (1992), pp. 6131-6140

[17] P.E. Hopkins, B. Kaehr, E.S. Piekos, D. Dunphy, C.J. Brinker

Minimum thermal conductivity considerations in aerogel thin film
J. Appl. Phys., 111 (2012)

[18] A.D. Caplin, C. Rizzuto

J. Phys. C Solid State Phys., 3 (1970), p. L117

[19] S. Latré, D. Seveno, F. Desplentere

Computational modeling of thermal phenomena in nanomaterials for building applications
D. Brabazon (Ed.), Reference Module in Materials Science and Materials Engineering(Reference Module in Materials Science and Materials Engineering). The Boulevard, Langford Lane, ELSEVIER, Kidlington, Oxford OX5 1GB, UK (2018)[

[20] M.G. Kaganer

Thermal Insulation in Cryogenic Engineering
Israel Program for Scientific Translations, Jerusalem (1969)

[21] J.J. Zhao, Y.Y. Duan, X.D. Wang, B.X. Wang **A 3-D numerical heat transfer model for silica aerogels based on the porous secondary nanoparticle aggregate structure** J. Non-Cryst. Solids, 358 (2012), 10.1016/j.jnoncrysol.2012.02.035

[22] O.J. Lee, K.H. Lee, T. Jin Yim, S. Young Kim, K.P. Yoo **Determination of mesopore size of aerogels from thermal conductivity measurements** J. Non-Cryst. Solids, 298 (2–3) (2002), pp. 287-292, 10.1016/S0022-3093(01)01041-9

[23] S. Lallich, F. Enguehard, D. Baillis **Experimental determination and modeling of the radiative properties of silica nanoporous matrices** J. Heat Tran., 131 (8) (2009), pp. 1-12 082701

[24] H. Yu, D. Liu, Y. Duan, X. Wang **Theoretical model of radiative transfer in opacified aerogel based on realistic microstructures** Int. J. Heat Mass Tran., 70 (2014), pp. 478-485
[26] F. Enguehard **Multi-scale modeling of radiation heat transfer through nanoporous superinsulating materials** Int. J. Thermophys., 28 (2007), pp. 1693-1717

[27] J. Wang, J. Kuhn, X. Lu **Monolithic silica aerogel insulation doped with TiO2 powder and ceramic fibers** J. Non-Cryst. Solids, 186 (1995), pp. 296-300

[28] T. Rettelbach, J. Sauberlich, S. Korder, J. Fricke **Thermal conductivity of IR-opacified silica aerogel powders between 10 K and 275 K** J. Phys. Appl. Phys., 28 (2010), pp. 581-587

[29] J.P. Feng, D.P. Chen, W. Ni, S.Q. Yang, Z.J. Hu**Study of IR absorption properties of fumed silica-opacifier composites** J. Non-Cryst. Solids, 356 (2010), pp. 480-483

[30] J.J. Zhao, Y.Y. Duan, X.D. Wang, B.X. Wang **An analytical model for combined radiative and conductive heat transfer in fiber-loaded silica aerogels** J. Non-Cryst. Solids, 358 (10) (2012), pp. 1303-1312 ArticleDownload PDFView Record in ScopusGoogle Scholar

[31] J.J. Zhao, Y.Y. Duan, X.D. Wang, B.X. Wang**Experimental and analytical analyses of the thermal conductivities and high-temperature characteristics of silica aerogels based on microstructures** J. Phys. Appl. Phys., 46 (1) (2013), 10.1088/0022-3727/46/1/015304

[32] J.S.Q. Zeng, R. Greif, P. Stevens, M. Ayers, A. Hunt**Effective optical constants n and κ and extinction coefficient of silica aerogel** J. Mater. Res., 11 (3) (1996), pp. 687-693

[33] G. Wei, Y. Liu, X. Zhang, F. Yu, X. Du **Thermal conductivities study on silica aerogel and its composite insulation materials** Int. J. Heat Mass Tran., 54 (11–12) (2011), pp. 2355-2366, 10.1016/j.ijheatmasstransfer.2011.02.026

[34] M.A. Aegerter, N. Leventis, M.M. Koebel **Aerogels Handbook** Springer-Verlag, New York (2011)

[35] A. Soleimani Dorcheh, M.H. Abbasi **Silica aerogel; synthesis, properties and characterization**J. Mater. Process. Technol., 199 (2008), pp. 10-26

[36] D. Dan, H. Zhang, W.Q. Tao **Effective structure of aerogels and decomposed contributions of its thermal conductivity**Appl. Therm. Eng., 72 (1) (2014), pp. 2-9, 10.1016/j.applthermaleng.2014.02.052

[37] J.J. Zhao, Y.Y. Duan, X.D. Wang, B.X. Wang**Effects of solid-gas coupling and pore and particle microstructures on the effective gaseous thermal conductivity in aerogels** J. Nanoparticle Res., 14 (8) (2012), 10.1007/s11051-012-1024-0

[38] Q. Fang, B. David **Tetrahedral mesh generation from volume tric binary and gray-scale images"** Proc. IEEE Int. Symp. Biomed. Imag. (2009), pp. 1142-1145

[39] E. Cuce, P.M. Cuce, C.J. Wood, S.B. Riffat **Toward aerogel based thermal superinsulation in buildings: a comprehensive review** Renew. Sustain. Energy Rev., 34 (2014), pp. 273-299, 10.1016/j.rser.2014.03.017